
STRUCTURE NOTE

Crystal Structure of *Homo sapiens* Protein hp14.5

Babu A. Manjasetty,^{1,2†} Heinrich Delbrück,^{3,4} Dinh-Trung Pham,^{4,5} Uwe Mueller,^{1,3} Martin Fieber-Erdmann,^{1,3} Christoph Scheich,^{4,6} Volker Sievert,^{4,6} Konrad Büssow,^{4,6} Frank H. Neisen,^{4,7} Wilhelm Weihofen,³ Bernhard Loll,³ Wolfram Saenger,³ and Udo Heinemann^{2,3*}

¹Protein Structure Factory, c/o BESSY GmbH, Berlin, Germany

²Forschungsgruppe Kristallographie, Max-Delbrück-Centrum für Molekulare Medizin, Berlin, Germany

³Institut für Chemie/Kristallographie, Freie Universität Berlin, Germany

⁴Protein Structure Factory, Berlin, Germany

⁵Alpha-Bioverfahrenstechnik GmbH, Kleinmachnow, Germany

⁶Max-Planck-Institut für Molekulare Genetik, Berlin, Germany

⁷Universitätsklinikum Charité, Institut für Medizinische Physik & Biophysik Berlin, Germany

Introduction. Human trichloroacetic acid-soluble protein p14.5 (hp14.5) is a member of the large YjgF/YER057c/UK114 protein family, which comprises approximately 200 members,¹ most with unclear biological function. The hp14.5 homologs belonging to the high-identity (>38%) group (approximately 80 proteins) share 9 completely invariant residues that are spread throughout the sequence.¹ The crystal structures of 3 distant homologs have been determined: YabJ from *Bacillus subtilis* (45% identity),² YjgF from *Escherichia coli* (46% identity),³ and Yeo7 from yeast (39% identity).⁴ These proteins share similar homotrimeric structures and distinct clefts located between the subunits that may be of functional relevance. Recently, the NMR structure of the homologous H10719 from *Haemophilus influenzae* (44% identity) has been determined.¹ Based on this structure, an NMR ligand screening was performed using a set of molecules related to the various cellular functions reported in the literature (i.e., translation inhibition,^{5,6} ribonuclease activity,⁷ and involvement in the regulation of purine⁸ and isoleucine⁹ biosynthetic pathways).

Human p14.5 was first isolated from mononuclear phagocytes.⁶ Using a rabbit reticulocyte lysate system, it was shown that recombinant hp14.5 in micromolar concentrations and native hp14.5 in nanomolar concentrations inhibit protein synthesis *in vivo*. Whereas the hp14.5 mRNA is weakly expressed in freshly isolated monocytes, it is upregulated when these monocytes differentiate to macrophages.⁶ Clear evidence for a differentiation-dependent regulation of hp14.5 synthesis is provided by the observation that in a variety of liver and kidney tumor cells, only a low expression level is observed, whereas in fully differentiated cells, a high level is measured.⁶ Inhibition of protein synthesis *in vitro*, similar to that observed for hp14.5, was described for the homologous rat perchloric acid-soluble protein (L-PSP).⁵ The translation-inhibitory activity of L-PSP has been attributed to its endoribonucleolytic activity toward single-stranded RNA,⁷ which induces

disaggregation of the reticulocyte polysomes into 80S ribosomes even in the presence of cycloheximide.

Results. Like several homologous YjgF/YER057c/UK114 protein family members, the human translational inhibitor protein, hp14.5, adopts a chorismate mutase-like^{3,10} subunit fold. Each monomer consists of one globular domain formed by a 6-stranded β -sheet and two α -helices arranged in roughly parallel orientation on one side of the sheet [Fig. 1(a)]. In the β -sheet, the order of strands from one edge to the other is 1-2-3-6-4-5, where β 4 and β 5 are in parallel and all other strands are antiparallel.

Three hp14.5 monomers associate into a trimer with threefold noncrystallographic symmetry [Fig. 1(b)]. Three such trimers formed by 9 polypeptide chains constitute the asymmetric unit of the crystal. Pairwise superpositions of the 3 trimers yield root-mean-square deviation (RMSD) values of 0.399 Å, 0.607 Å, and 0.556 Å, indicating closely related trimer organization. The shape of the trimer resembles a triangular barrel. Three pairs of α -helices are positioned on its outer surface, and 3×4 antiparallel strands form the inner surface of the barrel. The barrel is sealed off at one end by Tyr¹¹⁰ from each of the 3 subunits, and at the other end by 3 other tyrosines, Tyr³². The sealing of the barrel leads to the formation of a large cavity filled with water molecules. The biological role of this cavity, if any, is not clear. On the outer surface of the

Grant sponsor: German Federal Ministry for Education and Research (BMBF) through the "Leitprojektverbund Proteinstrukturfabrik." Grant sponsor: Fonds der Chemischen Industrie to Udo Heinemann and Wolfram Saenger.

*Correspondence to: Udo Heinemann, Max Delbrück Center for Molecular Medicine, Robert-Rössle-Str. 10, D-13092, Berlin, Germany. E-mail: heinemann@mdc-berlin.de

†On leave from the Department of Physics, Government Science College, Bangalore, India.

Received 13 August 2003; Accepted 14 August 2003

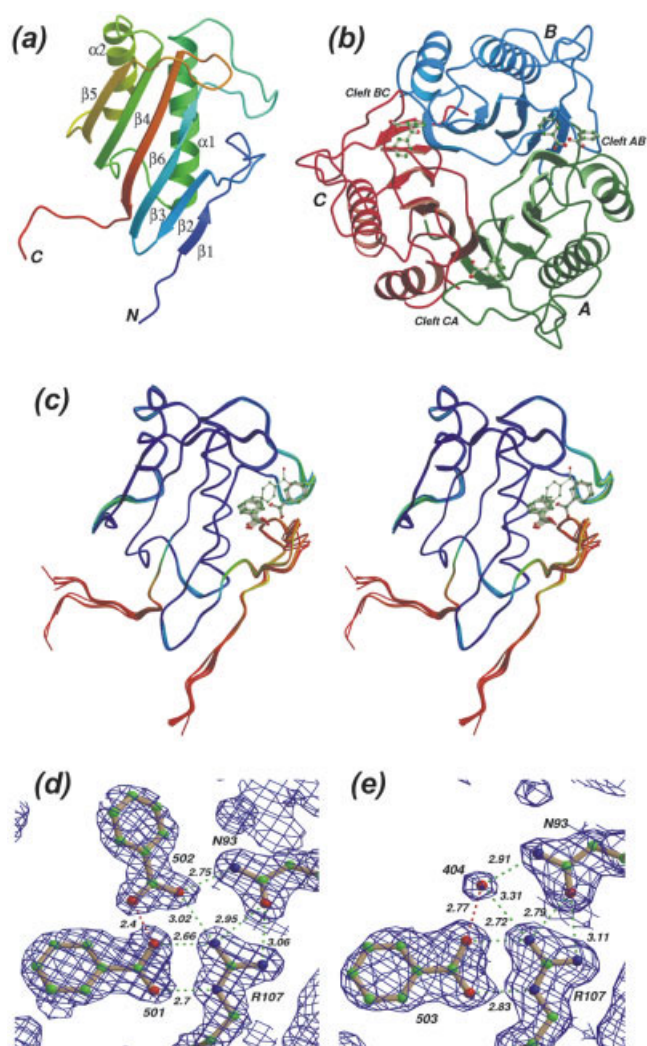


Fig. 1. (a) Ribbon diagram of hp14.5. The colors change smoothly from blue at the N-terminus to red at the C-terminus. (b) Hp14.5 trimer with benzoate molecules bound at the subunit interfaces. The view is along the noncrystallographic threefold symmetry axis. Subunits are drawn with different colors. The clefts at the subunit interfaces are labeled. (c) Least-squares superposition of all 9 hp14.5 monomers. The colors blue, green, orange, and red indicate mean temperature factors of 15, 25, 35, and 45 Å², respectively. Benzoate molecules binding to the protein are shown in ball-and-stick representation. (d and e) Electron density and ligand binding at clefts AB (d) and CA (e) of hp14.5. The well conserved interactions of the benzoate with the side-chains of the invariant residues Arg¹⁰⁷ and Asn⁹³ of hp14.5 are shown. The $2F_o - F_c$ electron density map is contoured at 1.1 σ .

trimer, the interfaces between adjacent subunits form 3 equivalent clefts—AB, BC, and CA—that are approximately 12 Å deep and 8 Å wide [Fig. 1(b)]. These clefts are formed by $\alpha 2$, $\beta 4$, and $\beta 5$ from one subunit and $\beta 3$, $\beta 5$, and the loop between $\beta 3$ and $\alpha 1$ from the adjacent subunit. The flexible loop between $\beta 1$ and $\beta 2$ from the adjacent subunit forms a cap-like structure over the cleft. The observed flexibility of this loop with elevated temperature factors and high RMSDs between the 9 monomers [Fig. 1(c)] suggest that the loop may be involved in modulating the geometry for ligand binding.

Like homologous proteins,^{1–4} hp14.5 displays high acid

stability. The unfolding of hp14.5 as a function of pH was monitored by differential scanning calorimetry (DSC; not shown). At all tested pH values, a single transition was observed, followed by a strong decrease in the heat capacity, indicating aggregation after thermal denaturation. A high stability of hp14.5 is revealed by the determined melting temperatures (T_m): At pH 7, hp14.5 shows a melting transition with $T_m = 88.6^\circ\text{C}$. At pH 6, the T_m was even higher, 93.6°C , whereas it was lowered to 84.4°C at pH 8. The observed DSC scans fit well to a monophasic melting transition, indicating the unfolding of hp14.5 in a two-state process.

In the hp14.5 structure, 7 out of the 9 strictly conserved residues of the high-identity group of YjgF/YER057c/UK114 proteins line the walls of the intersubunit cleft. Of these 7 residues, 3 (Phe⁸⁹, Asn⁹³, and Arg¹⁰⁷) belong to one subunit and 4 (Tyr²¹, Gly³⁵, Pro¹¹⁶, and Glu¹²²) to the other. The invariant residue Arg¹⁰⁷ is prominent and immediately accessible in the cleft. In all 9 hp14.5 intersubunit clefts observed in the asymmetric unit of the crystal, the Arg¹⁰⁷ guanidinium group is geometrically fixed by two short hydrogen bonds linking Nⁿ¹ and Nⁿ² to Asn⁹³ O^{δ1} from same subunit of the trimer. The carboxylate group of the invariant Glu¹²² is hydrogen-bonded to the protein backbone atoms of Ala¹⁰⁹ at strand $\beta 5$ of the other subunit and thereby helps seal the bottom of the cleft. The electron density for the invariant Phe⁸⁹ tends to be poorly defined, and the side-chain has different conformations in different clefts. Tyr²¹ has a similar conformation in all clefts with its hydroxyl group accessible to ligand interactions. Gly³⁵, which resides in an allowed region of the Ramachandran map ($\Phi = -60.4^\circ$ and $\Psi = 123.4^\circ$ for Gly³⁵ of chain A) may be conserved for structural reasons, because any mutation of Gly³⁵ will cause a steric clash of a C ^{β} atom with the Glu¹²² side-chain. Well-defined electron density is observed for Pro¹¹⁶ in all 9 copies, implying that this residue is rigidly placed within the cleft.

In these 9 clefts in the 3 hp14.5 trimers, a total of 13 benzoate molecules are bound to the protein in either 1:1 or 1:2 (protein to ligand) molar ratio, with similar but slightly different geometry [Fig. 1(b–e)]. A common mode of binding to a primary site is observed for one benzoate molecule in all 9 clefts, whereas a second benzoate is either absent (5 cases) or bound weakly and with different orientations to a secondary site. Primary-site binding is through interactions of benzoate with the side-chains of Arg¹⁰⁷ of one subunit and Tyr²¹ of another subunit. In this mode, the ligand is deeply buried within the cleft. The most striking protein–ligand interaction seen in all 9 clefts is the formation of strong bidentate salt bridges between the carboxylate oxygens O¹/O² of benzoate and Nⁿ²/Nⁿ¹ of the conserved Arg¹⁰⁷ as shown in Figure 1(d and e) for benzoates 501 and 503 bound to clefts AB and CA, respectively. An additional interaction with Tyr²¹ (not shown) is mainly between the π -system of the ligand's phenyl ring and the phenolic oxygen of the Tyr²¹ side-chain.

The secondary-site binding observed in some clefts of the hp14.5 trimer involves the Phe⁸⁹ and Pro¹¹⁶ side-chains,

again belonging to two different subunits, that sandwich the benzoate phenyl ring by Van der Waals interactions. In the AB cleft [see Fig. 1(d)], the benzoate molecule 502 is, in addition, engaged in hydrogen bonding to the protein (O^1 to Asn⁹³ N⁶² and Arg¹⁰⁷ N⁷²) and to benzoate-501. The short (2.4 Å) hydrogen bond between benzoate-502 O^1 and benzoate-501 O^2 requires the carboxy group of the former to be protonated at O^1 . Given the $pK_a = 4.2$ of benzoate in aqueous solution and the neutral pH of crystallization, this appears possible. A similar mode of benzoate binding is observed at two clefts in the other trimers, whereas benzoate binds differently to the secondary site of cleft BC [see Fig. 1(c)], where its carboxylate group is oriented outward from the protein. In the CA cleft, the position of the secondary site carboxylate group is occupied by water molecule 404 [Fig. 1(e)], which satisfies the hydrogen-bonding potential of binding-site residues left unfilled by the missing secondary benzoate.

There is no reason to assume that benzoate is the natural ligand of hp14.5. Rather, the benzoate-binding site may mark a functional site involved in the ribonucleolytic or a different activity of hp14.5. The relatively high concentration of sodium benzoate (300 mM) in the crystallization buffers allows the molecule to occupy a site tailored for binding of a chemically similar natural ligand. However, primary-site binding to the invariant Arg¹⁰⁷ has been clearly seen in crystals grown from 45 mM benzoate (not shown). This indicates that the protein is able to bind benzoate with a moderate dissociation constant.

The NMR structure of the bacterial homolog H10719 has served as the basis for an NMR-based ligand screening that was performed using a set of molecules related to the various cellular functions.¹ Six small ligands were identified, which are able to bind H10719. Strikingly, all these ligands are either α -keto acids or α,β -unsaturated acids, thus structurally resembling the benzoate ligands of hp14.5. Surprisingly, however, the chemical-shift changes indicated binding to Ser¹⁰⁸ instead of the invariant Arg¹⁰⁷ of H10719 for one of the tightest binders, 2-ketobutyrate.

Materials and Methods. A cDNA fragment corresponding to the open reading frame of hp14.5 (GenBank accession CAA64670) was amplified by polymerase chain reaction (PCR) from a cDNA clone from the I.M.A.G.E. Consortium¹¹ (I.M.A.G.E. Clone ID 323812). The PCR product was cloned into the vector pQTEV (GenBank accession AY243506), and the resulting plasmid was introduced into *E. coli* SCS1 cells carrying the helper plasmid pSE111 that provides resistance to 15 μ g/mL kanamycin and carries the *lacIQ* repressor and the *argU* gene for a rare tRNA. The resulting clone that was used for protein expression has the Protein Structure Factory (PSF) clone ID 104124, and is available from the German Resource Center (<http://www.rzpd.de>) under the identifier PSFEp758H0822.

The *E. coli* cells were subsequently fermented at 37°C in Superbroth (SB) medium containing 10 mg/mL kanamycin and 50 mg/mL ampicillin for 8 $\frac{1}{2}$ h. Gene expression was induced after 4 $\frac{1}{2}$ h by the addition of isopropyl- β -D-thiogalactopyranoside (IPTG) to a final concentration of

0.5 mM. The cells (25.3 g/L) were harvested by centrifugation at 4°C. Aliquots of cell paste were resuspended in 200 mL extraction buffer (20 mM Tris-HCl, pH 8.0, 300 mM NaCl, 0.5 mM ethylene diaminetetraacetic acid (EDTA), 1 mM phenylmethyl sulfonyl fluoride (PMSF), 2 mM 2-mercaptoethanol), and lysozyme was added. The cells were then disrupted by ultrasonic treatment in a chilling water bath and the suspension was centrifuged at 50,000 *g* for 45 min. The resultant crude extract was filtrated and applied to a TALON metal affinity column equilibrated with 20 mM Tris-HCl, 150 mM NaCl, 10 mM imidazole, pH 7.4. After a wash step, the protein was eluted with 200 mM imidazole in the same buffer. The histidine-tag was removed by incubation with Tobacco Etch Virus (TEV) protease (molar ratio 1:40 protease:substrate) at 4°C overnight. After centrifugation (5 min at 5000 *g*) and 5-fold dilution with 20 mM Tris-HCl, pH 7.4, the protein solution was applied to a POROS 20 HQ anion-exchange column equilibrated with the same buffer to which hp14.5 did not bind. The flow-through was applied to a POROS HS cation-exchange column under the same buffer conditions. Again, hp14.5 did not bind. The flow-through was concentrated in a 70 mL Vivacell under N₂-pressure. In the final step, the sample was applied to a Superdex 75 size-exclusion column and equilibrated with crystallization buffer (15 mM Tris-HCl pH 7.4, 150 mM NaCl, 0.1 mM EDTA, 2 mM dithiothreitol (DTT)).

For DSC, the protein was diluted at least 20-fold in buffers 1 (20 mM 2-(4-morpholino)ethane sulfonic acid (MES)-NaOH, pH 6.0, 150 mM NaCl), 2 (20 mM Na/K phosphate, pH 7.0, 150 mM NaCl), or 3 (20 mM Na/K phosphate, pH 8.0, 150 mM NaCl). Buffers were checked for temperature stability of their pH values. The DSC measurements were performed using a MicroCal VP-DSC calorimeter (MicroCal, LLC, Northampton, MA) at a rate of 1 K/min. The resulting scans were baseline-corrected and the transition temperatures (T_m) were calculated using the instrument software (MicroCal Origin 5.0).

For crystallization, the protein was concentrated to 12.8 mg/mL and conditions were screened by the sitting-drop vapor-diffusion technique using a 96-well Greiner plate at 293 K. Initial trials were carried out using in-house developed screens based on commercially available crystallization kits. All pipetting steps were done with semiautomated dispensing systems.¹² Crystals appeared within 3–7 days in a solution containing 2 M sodium malonate and 0.3 M sodium benzoate at pH 7.0. The crystals belong to space group P3₁21 with unit cell dimensions of $a = 154.2$ Å, $c = 104.6$ Å. The solvent content, assuming 9 molecules with a total molecular mass of 131 kDa in the asymmetric unit, was calculated to be 54% ($V_M = 2.8$ Å³/Da). A Hg derivative was prepared by soaking the crystals in artificial mother liquor containing 15 mM ethyl-Hg phosphate (EMP) for 30 min. A native data set and single-wavelength anomalous diffraction data at the Hg L_{III} edge from the EMP derivative were collected at 100 K on the MAR345 imaging plate detector at the BESSY (Berlin) beamline PSF-ID14.2. The data were processed using the program DENZO¹³ and scaled with SCALEPACK¹³ (Table I).

TABLE I. Crystallographic Data

	Native hp14.5	EMP-hp14.5
Data collection statistics ^a		
Resolution (Å)	1.9	2.3
Wavelength (Å)	0.98004	1.00883
Total reflections	754,078	1,282,607
Unique reflections	110,385	119,928
Completeness (%)	98.4 (94.4)	100.0 (100.0)
Average I/σ(I)	22.9 (2.3)	18.5 (3.5)
R(merge) (%)	8.1 (55.0)	12.0 (88.3)
Refinement statistics		
Resolution range (Å)		20–1.9
Total reflections used in refinement		104,822
Number reflections in R(free) set		5511
R factor ^b		0.185
R(free) ^c		0.216
RMSD bond lengths (Å)		0.013
RMSD bond angles (°)		1.542
Number of nonhydrogen atoms		9551
Average B factor (Å ²)		20.6
Ramachandran plot statistics		
Favorable (% and number of residues)		90.3 (938)
Additional (% and number of residues)		8.8 (91)
Generously allowed (% and number of residues)		1.0 (10)
Disallowed		0

^aStatistics for the highest resolution shell are given in parentheses.

^b $R = \sum_n |F_o(h) - k|F_c(h)| / \sum_n |F_o(h)|$

^cFree R factor was calculated using a 5% randomly selected subset of the total number of reflections.

The 9 mercury atoms (bound to the single Cys⁷¹ of the 9 molecules in the asymmetric unit) were located by the program SnB¹⁴ using the anomalous differences. The anomalous phasing and refinement of the Hg positions were done using the program Solve.¹⁵ The resulting electron density was subjected to solvent flattening and further improved by 9-fold noncrystallographic symmetry averaging, along with automatic model building and refinement with RESOLVE¹⁶ in combination with REFMAC,¹⁷ which yielded 948 out of 1242 residues. After phase extension to 1.9 Å resolution, the remaining residues were built manually with the program O¹⁸. Thirteen benzoate molecules were identified and included in the refinement. The final model consists of 1210 residues: 2–135 for 6 chains (B, C, D, E, F, G), 2–136 for 2 chains (H and I), and 2–137 for the remaining chain (A) plus 13 benzoate and 444 water molecules. For the 9 hp14.5 molecules in the asymmetric unit, TLS parameters were determined and translation, libration, screw-rotation (TLS) restrained refinement was performed.¹⁹ The final refinement statistics are shown in Table I. Atomic coordinates and structure factors are available from the PDB under accession code 1ONI. The hp14.5 structure was determined within the Protein Structure Factory.²⁰

Acknowledgments. We wish to thank Nabila Ibrahim, Anja Koch, Thomas Grund, Jannett Tischer, and Claudia Alings for technical assistance.

Note added in press: The structure of the homologous protein from goat was published after submission of this manuscript.²¹

REFERENCES

- Parsons L, Bonander N, Eisenstein E, Gilson M, Kairys V, Orban J. Solution structure and functional ligand screening of HI0719, a highly conserved protein from bacteria to humans in the YjgF/YER057c/UK114 family. *Biochemistry* 2003;42:80–89.
- Sinha S, Rappu P, Lange SC, Mäntsälä P, Zalkin H, Smith JL. Crystal structure of *Bacillus subtilis* YabJ, a purine regulatory protein and member of the highly conserved YjgF family. *Proc Natl Acad Sci USA* 1999;96:13074–13079.
- Volz K. A test case for structure-based functional assignment: The 1.2 Å crystal structure of the yjgF gene product from *Escherichia coli*. *Protein Sci* 1999;8:2428–2437.
- Deaconescu AM, Roll-Mecak A, Bonanno JB, Gerchman SE, Kycia H, Studier FW, Burley SK. X-ray structure of *Saccharomyces cerevisiae* homologous mitochondrial matrix factor 1 (Hmf1). *Proteins* 2002;48:431–436.
- Oka T, Tsuji H, Noda C, Sakai K, Hong YM, Suzuki I, Muñoz S, Natori Y. Isolation and characterization of a novel perchloric acid-soluble protein inhibiting cell-free protein synthesis. *J Biol Chem* 1995;270:30060–30067.
- Schmiedeknecht G, Kerkhoff C, Orso E, Stohr J, Aslanidis C, Nagy GM, Knuechel R, Schmitz G. Isolation and characterization of a 14.5-kDa trichloroacetic-acid-soluble translational inhibitor protein from human monocytes that is upregulated upon cellular differentiation. *Eur J Biochem* 1996;242:339–351.
- Morishita R, Kawagoshi A, Sawasaki T, Madin K, Ogasawara T, Oka T, Endo Y. Ribonuclease activity of rat liver perchloric acid-soluble protein, a potent inhibitor of protein synthesis. *J Biol Chem* 1999;274:20688–20692.
- Rappu P, Shin BS, Zalkin H, Mäntsälä P. A role for a highly conserved protein of unknown function in regulation of *Bacillus subtilis* *purA* by the purine repressor. *J Bacteriol* 1999;181:3810–3815.
- Kim JM, Yoshikawa H, Shirahige K. A member of the YER057c/yjgF/UK114 family links isoleucine biosynthesis and intact mitochondria maintenance in *Saccharomyces cerevisiae*. *Genes Cells* 2001;6:507–517.
- Chook YM, Ke H, Lipscomb WN. Crystal structures of the monofunctional chorismate mutase from *Bacillus subtilis* and its complex with a transition state analog. *Proc Natl Acad Sci USA* 1993;90:8600–8603.
- Lennon G, Auffray C, Polymeropoulos M, Soares MB. The I.M.A.G.E. Consortium: An integrated molecular analysis of genomes and their expression. *Genomics* 1996;33:151–152.
- Mueller U, Nyarsik L, Horn M, Rauth H, Przewieslik T, Saenger W, Lehrach H, Eickhoff H. Development of a technology for automation and miniaturisation of protein crystallisation. *J Biotechnol* 2001;85:7–14.
- Otwiowski Z, Minor W. Processing of X-ray diffraction data collected in oscillation mode. *Methods Enzymol* 1997;276:307–326.
- Miller R, Gallo SM, Khalak HG, Weeks CM. Snb—crystal structure determination via Shake-and-Bake. *J Appl Crystallogr* 1994;27:613–621.
- Terwilliger TC, Berendzen J. Automated MAD and MIR structure solution. *Acta Crystallogr D Biol Crystallogr* 1999;55:849–861.
- Terwilliger TC. Maximum-likelihood density modification using pattern recognition of structural motifs. *Acta Crystallogr D Biol Crystallogr* 2001;57:1755–1762.
- Murshudov GN, Vagin AA, Dodson EJ. Refinement of macromolecular structures by the maximum-likelihood method. *Acta Crystallogr D Biol Crystallogr* 1997;53:240–255.
- Jones TA, Zou JY, Cowan SW, Kjeldgaard M. Improved methods for building protein models in electron density maps and the location of errors in these models. *Acta Crystallogr A* 1991;47:110–119.
- Winn MD, Isupov MN, Murshudov GN. Use of TLS parameters to model anisotropic displacements in macromolecular refinement. *Acta Crystallogr D Biol Crystallogr* 2001;57:122–133.
- Heinemann U, Büsow K, Mueller U, Umbach P. Facilities and methods for the high-throughput crystal structure analysis of human proteins. *Acc Chem Res* 2003;36:157–163.
- Deriu D, Briand C, Mistiniene E, Naktinis V, Grütter MG. Structure and oligomeric state of the mammalian tumour-associated antigen UK114. *Acta Crystallogr D Biol Crystallogr* 2003;59:1676–1678.